CONFERENCE PROCEEDINGS

September 27-29, 2024

Victoria, Canada

GLOBAL CONFERENCE ALLIANCE INC. ™
www.globalconference.ca
Proudly Canadian, Truly Global

Conference Proceeding

September 27-29, 2024 - Victoria, Canada

Format: Electronic Book

ISBN: 978-1-998259-50-2

Table of Contents

Content Details:

Avninder Gill (Author) *Thompson Rivers University*	**Embedding Expert Knowledge in Supply Chain Project Decisions.**

Abstract

Making effective supply chains decisions and successfully bidding on operational projects requires a certain degree of precision in estimating the costs of such decisions. However, the factors that contribute to the cost are based on the managerial and expert knowledge and cannot often be determined with a high degree of accuracy. Fuzzy logics provides a viable option to model such scenarios. The present paper explores the use of fuzzy linguistic approach to embed expert knowledge and judgement in costing decisions. The methodology and the model is explained with the help of an illustrative example.

Keywords: Supply Chain Management; Expert Knowledge; Project Costing; Fuzzy Logics

Charles Kusi (Author)
Sheckles Investments Ventures

Saeed Debrah Opoku (Co-Author)
Sheckles Investments Ventures

A Granger Causality-Panel Regression Analysis of the Nexus of Country Risk and FDI From Emerging Economies: Evidence from Africa.

Abstract

This study sought to find the effect of country risk on foreign direct investments by measuring the impact of country risk on foreign direct investments and investigating the causality between the two.
The study adopted the quantitative approach and collected annual data spanning 1991 to 2020 on country risk scores of African countries from the International Country Risk Guide database as well as foreign direct investment net-inflows for African countries from the World bank's database of World Development Indicators.
Panel data modelling techniques were employed, and diagnostics tests indicated that the fixed effects model with individual as well as time effects was the appropriate panel model to use to analyze the data at hand.
The estimated fixed effects model as well as the panel Granger causality tests indicated that country risk causes foreign direct investment net-inflows and that countries with higher country risk ratings lose or gain more if their country risk ratings reduce or increase as the case may be, than countries with lower country risk ratings for the same amount of change in country risk ratings.
The study recommended that policy makers interested in attracting more FDI net-inflows should deliberately put in place policies and measures in the political, financial, and economic spheres that improves the country risk perception of their country since this will cause FDI net-inflows to increase.

Keywords: Foreign direct investments; Country risk; Granger causality.

1. Introduction

The phenomenon of Foreign Direct Investment (FDI) goes beyond international portfolio diversification, as it involves foreign companies owning more than 10% of a local company. FDI offers various benefits such as export diversification, access to foreign markets, expertise transfer, and technology transfer, making it highly sought after by developing countries (Kusek & Silva, 2017).

However, the uncertainties associated with doing business in foreign countries are captured through country risk scores, which encompass economic risk, transfer risk, exchange rate risk, location risk, sovereign risk, and political risk (Meldrum, 2000). Economic risk relates to unexpected changes in a country's economy affecting returns on investments, while transfer risk involves restrictions on capital movement. Exchange rate risk pertains to adverse exchange rate fluctuations, location risk considers spillover risks, and political risk involves political changes adverse to investments (Brown, Cavusgil, & Lord, 2015). Sovereign risk, in particular, relates to all these risks in country risk analysis.

Country risk scoring is a way to assess potential risks associated with cross-border investments (Koepke, 2019). These scores rely on expert opinions and quantitative indicators, with the International Country Risk Guide (ICRG) being a widely used source. The final numerical risk score reflects a country's overall risk profile.

This study aims to analyze the relationship between ICRG country risk scores and FDI flows in African countries over time, focusing on how these two factors interact in emerging markets.

FDI benefits are not guaranteed, and policies in host countries can impact their potential positive effects. Policies related to taxation, regulations, and political uncertainties can pose latent risks, including creeping expropriation (Sârbu, 2014; Koepke, 2019). Historical data shows that a significant portion of FDI to developing countries from 1956 to 1972 was expropriated without compensation (Williams, 1975).

Most existing research on FDI and country risk fails to investigate causality between the two. This study aims to delve deeper into the causal relationship between FDI and country risk and explore how one influences the other. The research's purpose is to determine the optimal level of country risk that is conducive for FDI. This study seeks to understand how country risk affects FDI flows, as a complete absence of risk is counterproductive to the risk-reward maxim. The overarching objective is to measure the impact of country risk on FDI, investigate causality between these variables, and assess the significance of country risk in attracting foreign direct investments.

Given that Foreign Direct Investment (FDI) plays a crucial role in the economic development of emerging economies, and it has become a prominent driver of growth and transformation in many African countries. Understanding the determinants and implications of FDI in these economies is vital for policymakers, businesses, and investors.

One of the primary motivations for this study is the increasing interest and importance of emerging markets, particularly in Africa, as attractive destinations for FDI. African nations are actively seeking to attract foreign investment to boost their economic development, employment opportunities, and infrastructure. However, the decision to invest in these countries is often influenced by various forms of risk, including political, economic, and social factors. It is imperative to investigate the extent to which country risk impact FDI inflows into African economies and whether these risks are perceived as significant obstacles by potential investors.

Furthermore, the study is motivated by the need to contribute to the existing literature on FDI and country risk, especially in the context of emerging economies. The unique economic, social, and political characteristics of African nations present an interesting and underexplored field of study. By focusing on this region, the research can shed light on the specific challenges and opportunities that investors face when considering FDI in African countries.

The outcomes of this study have practical implications for various stakeholders. Governments in African countries can gain insights into the factors that deter or attract FDI, enabling them to formulate policies that enhance their attractiveness to foreign investors. Businesses and multinational corporations can benefit from a better understanding of the risks involved in these markets and make more informed investment decisions. Additionally, investors can use the findings to evaluate the risk-return trade-offs when considering FDI opportunities in Africa.

2. Literature Review

The literature on Foreign Direct Investment (FDI) encompasses micro and macro theories, which have given rise to various sub-theories (Frenken & Mbuvi, 2017). The five-stage FDI or Investment Development Path (IDP) theory, which combines micro and macro elements, is particularly relevant in understanding the relationship between sovereign risk and FDI. This theory highlights the interplay between a country's economic development, measured by GDP per capita, and its net outward investment, defined as the difference between gross net outward investment and inward direct investment. It underscores the significance of economic structural changes and their systematic connection to FDI flows (Frenken & Mbuvi, 2017). Foreign investors engage in FDI to gain ownership or locational advantages, often driven by factors like stable economic and political environments, low production costs, and favorable tax regimes. Sovereign risk plays a crucial role in assessing locational advantage (Frenken & Mbuvi, 2017).

Jaiblai and Shenai (2019) expatiate four major FDI theories, including the product cycle theory, the eclectic paradigm theory, the perfect capital theory, and the internationalization theory. The product cycle theory outlines a four-stage production cycle: innovation, growth, maturity, and decline. Firms typically invest in foreign markets during the maturity stage when competition is intense, and they start exporting their products to foreign countries (Jaiblai & Shenai, 2019). The eclectic paradigm theory emphasizes three main factors motivating FDI: locational advantages, ownership advantages, and internationalization, which aligns with the IDP theory (Frenken & Mbuvi, 2017). The perfect capital theory, also known as the exchange market theory, suggests that changes in the real exchange rate impact export competitiveness, with a lower rate favoring exports (Jaiblai & Shenai, 2019). The internationalization theory, attributed to Hymer (1972), asserts that multinational enterprises engage in FDI to reduce competition and leverage their unique advantages, emphasizing that FDI is a firm-level strategic decision rather than a capital-market financial decision, with the aim of expanding market share (Jaiblai & Shenai, 2019; Kozlowska, 2015).

The concept of risk is defined differently by economists, scientists, risk theorists, and statisticians based on their specific contexts. Generally, risk is described as the uncertainty related to potential losses, as per Rejda (2014). This uncertainty forms the foundation of risk, but in finance and economics, authors often distinguish between uncertainty and risk. Uncertainty typically pertains to situations where the probability of an outcome cannot be estimated, while risk is used when the probability of an occurrence can be estimated with some accuracy. Systematic risk, stemming from external factors beyond a company's control, affects an entire economy or large groups of individuals and cannot be reduced through diversification (Topal & Gul, 2016). In contrast, nonsystematic risk, also known as particular risk, affects smaller groups and can be reduced through diversification. Examples of nonsystematic risk include fire, theft, and robbery, while systematic risk includes rapid inflation, earthquakes, and cyclical unemployment (Rejda, 2014). Sovereign risk is a subset of systematic risk, and it is associated with a government's inability or unwillingness to fulfill its debt obligations (Castro and Mencia, 2014; Zhang, 2010).

Sovereign risk can lead to the need for governments to issue new bonds to refinance existing debt, resulting in refinancing risk (Ali and Raza, 2014). Economic crises can exacerbate sovereign risk, making it more challenging for governments to repay their debt, as seen during the global financial crisis of 2007. In such cases, governments may need to rescue struggling banks, which can lead to an increase in sovereign default risk (Bruha and Kocenda, 2017). This interaction between banking and sovereign risk has been studied by various authors, including Zhang (2010).

Foreign Direct Investment (FDI) plays a crucial role in the development of many economies, particularly in the African region, which requires significant capital to finance their operations (Jaiblai & Shenai, 2019). FDI represents long-term investments by foreign investors in an economy or enterprise, offering benefits such as job creation, skill development, and enhanced local production (Jaiblai & Shenai, 2019). This type of investment provides stability during financial crises (Loungani and Razin, 2001). Furthermore, FDI contributes to an increase in corporate tax revenue and human capital development (Loungani and Razin, 2001; Sichei and Kiyondo, 2012).
Research shows a significant increase in global FDI inflows over the years, although there have been fluctuations due to events like the global financial crisis (Jaiblai & Shenai, 2019; Sichei & Kiyondo, 2012). Developing economies receive a substantial share of FDI inflows, but African countries receive a smaller share compared to other regions (Jaiblai & Shenai, 2019; Sichei & Kiyondo, 2012). In 2017, Africa received about 6% of total FDI inflows to developing countries, with Ghana, Nigeria, Ethiopia, Egypt, and Morocco being the top five recipients in the region (Jaiblai & Shenai, 2019).

FDI in Africa takes the form of efficiency-seeking, market-seeking, and resource-seeking investments (Jaiblai & Shenai, 2019). Additionally, Sichei and Kiyondo (2012) categorized FDI into market-seeking, asset-seeking, and efficiency-seeking types. Iloie (2015) classified FDI into mergers and acquisitions, firm restructuring, business development, and Greenfield investment, based on the nature of the investment.

In the realm of investment decision-making, Kozłowska (2015) has identified two primary classifications of risk in the context of foreign investments: general risk and special risk, which is also referred to as international investment risk. General risk pertains to overall investment, while special risk is associated with the geographical location of the investment outside the investor's home country. Special risk encompasses political and economic aspects but lacks a universally accepted definition. Topal and Gul (2016) support these notions and highlight three key factors influencing special or international investment risk: the competitive environment, macroeconomic conditions in the host country, and business risk.

Special risk further comprises political and economic components, with political risk arising from information asymmetry about political relations and changes in the foreign country and encompassing a lack of information about social, legal, religious, and cultural factors in the host country. Economic risk is rooted in foreign investors' insufficient knowledge of the economic situation in the foreign country, especially affecting those heavily reliant on raw materials and low labor costs within the host country (Jaiblai and Shenai, 2019). Foreign investors dependent on the macroeconomic situation in the host country face higher economic risk, with various microeconomic factors also posing potential risks. These microeconomic factors include exchange rates, inflation levels, taxes, interest rates, and local laws, which can all disrupt foreign investment operations. For example, exchange rate fluctuations introduce instability and uncertainty in cost and investment returns for foreign investors (Kozłowska, 2015).

The research by Jaiblai and Shenai (2019) investigates the determinants of Foreign Direct Investment (FDI) in Sub-Saharan economies from 1990 to 2017, highlighting the role of economic factors such as inflation, market size (measured by GDP), openness, and exchange rates in attracting FDI. High inflation is associated with lower FDI inflows, as it increases investment risk, consistent with Kozlowska (2015). On the other hand, Omankhanlen (2010) suggests that inflation has no significant effect on FDI in Nigeria, with foreign exchange rates being a more critical factor.

Market size, according to Jaiblai and Shenai (2019) and Sichei and Kiyondo (2012), plays a pivotal role in attracting FDI. Asiedu (2006) supports this, pointing out that FDI in Sub-Saharan Africa is primarily driven by natural resources and market size, with South Africa, Angola, and Nigeria receiving significant FDI due to large local markets and abundant natural resources.

Kozlowska (2015) explains that factors like legal systems, resource management, and inflation impact investment risk and FDI attractiveness, with more stable economies attracting higher FDI. Political stability and judicial improvements have also made Africa an appealing investment destination (KPMG, 2016).

Sichei and Kiyondo (2012) reveal that natural resources, real GDP growth, agglomeration economies, and domestic/international FDI policies are key determinants of FDI in Africa, consistent with Asiedu's findings. Agglomeration economies have the most significant influence on FDI, and natural resources attract resource-seeking investors.

Before 1950, investors focused on returns with little concern for risk, but after 1950, risk awareness increased. Sovereign risk emerged as a key concern for foreign investors, with factors like per capita income, GDP, and macroeconomic indicators influencing sovereign risk (Cantor & Packer, 1996; Ali & Raza, 2014). Country risk, a broader concept, encompasses economic, sovereign, political, exchange, capital, and neighborhood risks (Savoiu & Ciuca, 2013). Mateev and Stoyanov (2014) highlight that market size, low labor costs, trade barriers, and market growth prospects influence FDI inflows in Bulgaria.

Research on country risk's impact on FDI (Al-Samman & Mouselli, 2018; Rodriguez, 2016; Topal & Gul, 2016; Mateev & Stoyanov, 2014; Savoiu & Ciuca, 2013) suggests that political stability, regulatory quality, and absence of violence influence FDI. Topal and Gul (2016) find a positive relationship between decreased political and economic risk and FDI in developing countries.

Petrovic and Stankovic (2009) emphasize that country risk involves sovereign and transfer risks, with sovereign risk significantly affecting FDI. However, Iloie (2015) argues that the impact of FDI on host countries varies, influenced by social, political, economic, and institutional factors, challenging the idea of a strong link between sovereign risk and FDI. Hayakawa, Kimura, and Lee (2013) assert that only political risk affects FDI inflows.

Most research combines country risk and sovereign risk, but this paper uniquely focuses on FDI in Africa and its relationship with sovereign risk. The decline in Africa's share of FDI inflows is a significant concern, and this study seeks to clarify the specific role of sovereign risk in influencing FDI inflows to Africa.

3. Methodology

Previous research looking at the relationship between FDI and other variables have traditionally adopted the quantitative approach. The variables of this study (FDI and Country Risk Ratings) are measured as discrete quantitative data, and we seek interpretation of relationship and further make claims between these variables through numbers (parameter values) hence the quantitative approach is used in this study.

The data for the study is a panel made up of timeseries of foreign direct investments amounts to African countries at an annual frequency obtained from the World Development Indicators database of the World Bank Group as well as annual country risk scores of African countries obtained from the ICRG database. The data is obtained for the years spanning 1991 to 2020.

Two variables are used for this study, and they are foreign direct investment net inflows (FDI) and country risk scores (CRS).

FDI – the FDI variable is measured as net inflows and it is the value of inward direct investment made by non-resident investors in a reporting economy, including reinvested earnings and intra-company loans, net of repatriation of capital and repayment of loans. It is measured in US Dollars.

CRS – the ICRG composite scores is used as a measure of country risk for this study. ICRG is an online community of economic and political experts that provides real time scores in categories that relate to economic, structural, and political risk. The consensus expert scores, combined with scores on country borrowers' access to international capital markets, together with data from the IMF/ World Bank on debt indicators, create the ICRG composite country risk score.

According to Howell (2011) “the International Country Risk Guide (ICRG) rating comprises 22 variables in three subcategories of risk: political, financial, and economic. A separate index is created for each of the subcategories. The Political Risk index is based on 100 points, Financial Risk on 50 points, and Economic Risk on 50 points. The total points from the three indices are divided by two to produce the weights for inclusion in the composite country risk score. The composite scores, ranging from zero to 100, are then broken into categories from Very Low Risk (80 to 100 points) to Very High Risk (zero to 49.9 points)” (Howell, 2011). The score is displayed on a 100-point scale, with 100 being nearly devoid of any risk, and 0 being completely exposed to every risk.

Greene (2003) contends that the fundamental advantage of a panel data set is that it allows the researcher greater flexibility in modelling differences in behavior across individuals while Awunyo-Victor and Badu (2012) further buttress Greene (2003) point by observing that panel data facilitates identification of effects that cannot be detected using purely cross-section or timeseries data. Therefore, given that the data for the study is panel data, the analysis conducted via the panel data model of Verbeek (2004) given in general form as

$$y_{it} = \alpha + x_{it}^{'}\beta_{it} + \varepsilon_{it} \qquad (1)$$

where x_{it} is a k-dimensional vector of explanatory variables not including a constant and the α_i captures the effects of those variables that are peculiar to the i-th individual and that are constant over time, while the ε_{it} is assumed to be independent and identically distributed over individuals and time with a mean of zero and variance σ_{ε}^{2} in the standard case (Verbeek, 2004).

According to Judge, Hill, William, Lütkepohl and Lee (1982), we have a fixed effect model (FEM) if it is assumed that differences in the intercept parameter α_i captures all individual differences. On the other hand, we have the random effects models (REM) if apart from assuming that all individual differences are captured by the intercept parameters, we also recognize that the individuals in the sample were randomly selected with a definite mean μ and variance σ_{α}^{2}. The error term in the random effects model has two components: a time-invariant component and a remainder component that is uncorrelated over time.

Following the general panel model, the model used to achieve the first objective of the study is fashioned after the model of Ramcharran (1999) who conducted a similar study to this one. The model for this study is given as

$$FDI_{i,t} = \mu + \Phi SRS_{i,t} + \varepsilon_{i,t};\ E[\varepsilon_{i,t}] \sim N(0, \sigma^{2}) \qquad (2)$$

where

$FDI_{i,t}$ is the natural logarithm of FDI net inflow into country i at time t

$CRS_{i,t}$ is the country risk score for country i at time t

Φ is a parameter to be estimated and interpreted as the marginal impact of CRS on FDI.

μ is the intercept of the regression.

$\varepsilon_{i,t}$ is random error term made up of time-invariant but individual-variant errors, time-variant but individual invariant errors as well as a part that is both time and individual variant.

Model diagnostics is conducted via the Hausmann test and the Breusch and Pagan Lagrange Multiplier Test.

Baltagi (2005) notes that the Hausmann test provides a statistical basis for choosing between the fixed effects model (FEM) and the random effects model (REM) when it comes to estimating panel data regression models. The choice between the FEM and the REM is occasioned by the nature of correlation between the error terms and the explanatory variables. In the case where the error terms in the panel model are correlated with the explanatory variables the REM is consistent and efficient, but the FEM is only consistent but not efficient but in the case where the error terms are correlated with the explanatory variables then the FEM is both consistent and efficient whereas the REM is not consistent (Johnston & Dinardo, 1997). Gujarati (2004) indicates that the null hypothesis of the Hausmann test implies that REM and FEM estimators do not statistically differ substantially and that if the null hypothesis is rejected then the conclusion is that the REM is not appropriate, and the FEM is the better model to employ.

The Breusch and Pagan Lagrange Multiplier (BPLM) test is conducted to ascertain if specific effects are significant in a panel model. These specific effects are either individual effects, time effects or both. The two-way BPLM test statistically tests whether individual and time effects are significant in the model. The null hypothesis of this test indicates that specific effects (individual and time effects) are not significant in the model. Failure to reject the null hypothesis indicates that the pooled ordinary least squares (OLS) model is consistent and is preferred over the FEM. A rejection of the null hypothesis indicates the presence of specific effects and the choice of the FEM over the OLS as the best model to employ.

Panel Granger Causality Testing is employed to ascertain the direction of influence (if any among the variables of the study. CRS is said to Granger-cause FDI if FDI can be better predicted using the histories of both CRS and FDI than if it can by using the history of FDI alone. In the same vein, FDI is said to Granger-cause CRS if CRS can be better predicted using the histories of both FDI and CRS than if it can by using the history of CRS alone. The null hypothesis for the test indicates absence of causality therefore a rejection of the null hypothesis at the significance level of the test, indicates Granger causality in the direction tested while failure to reject the null hypothesis concludes that there is no causality in the direction being tested.

4. Results and Discussions

4.1 Summary Statistics

Table 1. Summary Statistics of Data

Var	Obs	Mean	Std. Dev.	Min	Max
FDI	1120	18.71	2.32	9.21	23.17
CRS	1120	58.31	11.65	13.75	84.48

Source: Author's evaluations,

The number of African countries contained in the data is 37 and the panel is unbalanced. It is noted from Table 1 that the mean of the FDI variable is 18.71 and this indicates that the mean net FDI inflow to the countries over the period of the study was $e^{18.71}$ or 133,551,803 US Dollars with the least net FDI inflow recorded being $e^{9.21}$or 9,997 US Dollars and the highest net FDI inflow recorded being $e^{23.17}$or 11,550,562,800 US.
Dollars. The mean CRS is 58.31 indicating that on average the countries in the dataset had a composite risk score of 58.31% from the ICRG over the period of the study with the maximum score being 84.48% and the minimum score being 13.75%.

4.2 Estimated Model

Six panel data models were fitted to the data, that is a fixed effect model (FEM), a random effect model (REM) and an ordinary least squares (OLS) model all without time and country effects while another set of the same models FEM, REM and OLS were estimated with time and country effects and the results are as summarized in Table 4.2 below. It is observed that the coefficients of all the models are significant at the 1% significance level indicating that the coefficients have passed the significance test at the default 5% level of testing too.

Table 2: Estimated Models

VARIABLES	(1) Fixed Effect	(2) Random Effect	(3) OLS	(4) Fixed Effect	(5) Random Effect	(6) OLS
CRS	0.142***	0.137***	0.0964***	0.0494***	0.0501***	0.0582***
	(0.0135)	(0.0127)	(0.00568)	(0.0128)	(0.0118)	(0.00575)
Constant	10.43***	10.74***	13.09***	14.06***	14.04***	14.29***
	(0.786)	(0.805)	(0.352)	(0.708)	(0.741)	(0.521)
Time Effects	No	No	No	Yes	Yes	Yes
Country Effects	No	No	No	Yes	Yes	Yes
Observations	1,120	1,120	1,120	1,120	1,120	1,120
R-squared	0.318		0.216	0.596		0.424
Number of ccodes	37	37		37	37	

Robust standard errors in parentheses

*** p<0.01, ** p<0.05, * p<0.1

4.2.1 Model Diagnostics

Table 3: Hausman (1978) test results

	Coef.
Chi-square test value	11.154
P-value	0.001

Source: Author's evaluations.

The Hausman (1978) specification test results (Table 3) indicates that the null hypothesis of no significant difference between the fixed effects model and random effects model is rejected in favour of the alternative hypothesis that the fixed effects model is the best model for the panel data of the study. This narrows the choice of models to either model (3) or (4) from Table 4.2 above but the Breusch and Pagan Lagrange multiplier test results (as shown in Table 4.3 below) indicates that the null hypothesis of no significant specific effects is rejected in favour of the alternative hypothesis; therefore, the conclusion is that the FEM is preferred over the OLS since there are significant individual and/or time effects.

Table 4: Breusch and Pagan (1980) Lagrange Multiplier Test Results

	Coef.
Chi-square test value	2331.3
P-value	0.0000

Source: Author's evaluations.

The results of the diagnostics tests on the models therefore indicate that the fixed effects model with individual and time effects is the model of choice for the panel data of the study and this is indicated by model (4) in Table 4 above.

4.2.2 Estimated Relationship between FDI and CRS

From the foregoing, the estimated equation for the panel data of the study is given as:

$$FDI = 14.06 + 0.0494CRS$$

This model can be interpreted as the FDI variable increases by 0.0494 units if the CRS variable increases by one unit.

But since $FDI = log(FDI\,net - inflow)$, the above model can be rewritten in terms of FDI net-inflow as:

$$log(FDI\,net - inflow) = 14.06 + 0.0494CRS$$

or

$$FDI\,net - inflow = e^{14.06+0.0494CRS}$$

This model shows that the marginal effect of country risk rating (CRS) on FDI net-inflow in Africa is dependent on the level of the country risk rating to begin with, thus a country with a lower country risk rating will experience a lower change in FDI net-inflow for a unit change in its country risk rating than a country with a higher country risk rating. This relationship for this model is as shown in Figure 1.

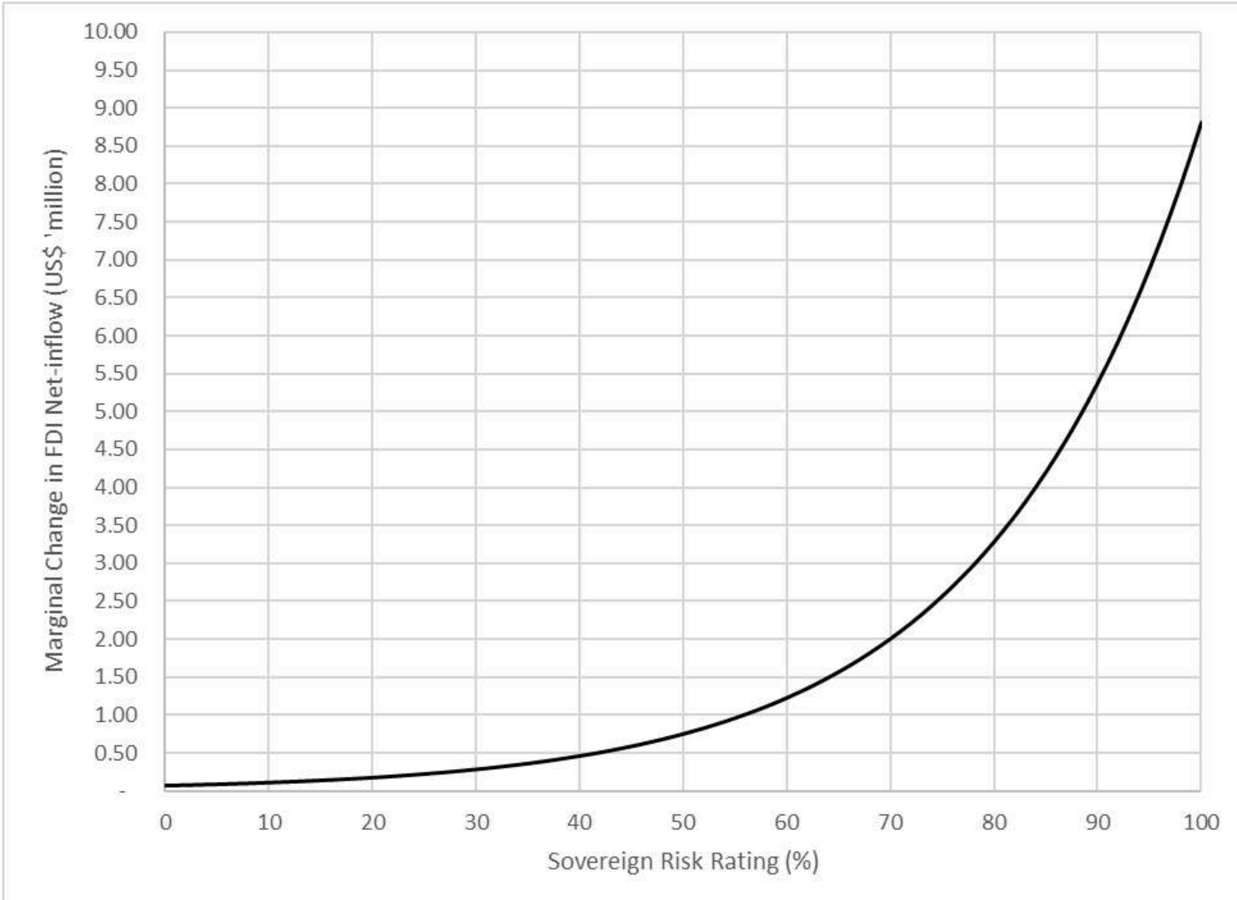

Figure 1: Marginal Change in FDI Net-Inflow Relative to Country Risk Rating

Table 5: Dumitrescu/Hurlin (2012) Panel Granger Causality Test Results Summary

Null Hypothesis	Obs.	Test at Lag 1 P-value	Test at Lag 2 P-value	Test at Lag 3 P-value
CRS does not Granger Cause FDI	1120	0.0000	0.0000	0.0000
FDI does not Granger Cause CRS		0.2935	0.3842	0.7113

Source: Author’s evaluations.

4.3 Granger Causality Test Result

The Dumitrescu/Hurlin (2012) panel Granger causality test was conducted at the first, second and third lags of the variables and the summary of the results is as shown in Table 5.
It is observed from Table 5 that the null hypothesis that CRS does not Granger cause FDI is rejected for all the lags at which the test was conducted because the p-value(s) is less than 5% (the level of significance of the test) and therefore the conclusion is that CRS Granger causes FDI.

On the other hand, there is a failure to reject the null hypothesis that FDI does not Granger cause CRS because the p-value(s) is greater than the significance level of the test (5%) and therefore the conclusion is that FDI does not Granger cause CRS.

Hence there is a unidirectional Granger causality from country risk rating to FDI net-inflow for countries in Africa. This buttresses the earlier finding that the marginal amount of FDI net flows to countries in Africa is dependent on their perceived country risk.

5. Conclusion

This study has found that country risk ratings significantly influence foreign direct investment net-inflows into Africa such that higher rating causes higher FDI net-inflows. This indicates that country risk ratings play a major role in the decisions of multinational entities as well as international investors in investing in Africa and given the fact that country risk ratings are a composite of political and economic perceptions of countries, it behoves any African country desiring more FDI net-inflows to put in measures that will make such a country to be perceived as improving the factors that go into the country risk ratings such as perception of the political atmosphere as well as the economic regimes. The study has shown that monotonically increasing FDI net-inflows is possible as long as country risk ratings are improving.

The study recommends that policy makers interested in attracting more FDI net-inflows should deliberately put in place policies and measures in the political, financial, and economic spheres that improves the country risk perception of their country since this will cause FDI net-inflows to increase. It is further recommended that this study be extended to compare the interactions found here in different contexts such as in developed, developing and under-developed countries and also disaggregate the components of country risk ratings (into political, financial, and economic factors) to find which factor matters most in directing FDI net-inflows.

Conflict of Interest Declaration

The authors declare no conflict of interest in the preparation of this manuscript.

References

Ali, J., & Raza, W. (2014). Analysis of Determinants of Sovereign Risk of Pakistan. *International Journal of Research & Development in Technology and Management Science-KAILASH*. 21(3): 90 – 99.

Al-Samman, H., & Mouselli, S. (2018). Does Country Risk Affect FDI to GCC Countries? *Pertanika Journal of Social Sciences & Humanities*, 26(4): 2627 – 2642.

Asiedu, E. (2006). Foreign direct investment in Africa: The role of natural resources, market size, government policy, institutions and political instability. *World economy*, 29(1), 63-77.

Awunyo-Vitor, D. and Badu, J. (2012). Capital structure and performance of listed banks in Ghana. *Global Journal of Human Social Science*, 12(5), pp.57-62.

Baltagi, B.H. (2005). *Econometric Analysis of Panel Data* (3rd ed.). UK: Wiley & Sons Ltd.

Bouchet, M. H., Fishkin, C. A., & Goguel, A. (2018). Managing Country Risk in an Age of Globalization: A Practical Guide to Overcoming Challenges in a Complex World. Springer.

Brown, C. L., Cavusgil, S. T., & Lord, A. W. (2015). Country-risk measurement and analysis: A new conceptualization and managerial tool. *International Business Review*, 24(2), 246-265.

Brůha, J., & Kočenda, E. (2017). Financial stability in Europe: Banking and sovereign risk. *Journal of Financial Stability*, 36, 305-321.

Cantor, R., & Packer, F. (1996). Determinants and Impact of Sovereign Credit Ratings. *Frbny Economic Policy Review*, 18.

Castro, C., & Mencia, J. (2014). Sovereign Risk and Financial Stability. *Revista de Estabilidad Financiera,* 26: 73- 107.

Frenken, J. H., & Mbuvi, D. (2017). Country risk, FDI flows and convergence trends in the context of the Investment Development Path. UNU-MERIT Working Papers, 5, 1-17.

Greene, W.H. (2003). *Econometric Analysis* (5th ed.). New Jersey: Pearson Education, Inc.

Gujarati, D.N. (2004). *Basic Econometrics* (4th ed.). New York: The McGraw-Hill Companies.

Hayakawa, K., Kimura, F., & Lee, H. H. (2013). How does country risk matter for foreign direct investment? *The Developing Economies*, 51(1), 60-78.

Howell, L., D. (2011). International Country Risk Guide Methodology. The PRS Group, Inc.

Hymer, S. (1972). Internationalization of Capital. *Journal of Economic Issues*, 6: 91–111

Iloie, R. E. (2015). Connections between FDI, corruption index and country risk assessments in Central and Eastern Europe. *Procedia Economics and Finance*, 32, 626-633.

Jaiblai, P., & Shenai, V. (2019). The Determinants of FDI in Sun-Saharan Economies: A Study of Data from 1990-2017. *International Journal of Financial Studies*, 7(43):1-31.

Johnston, J. and Dinardo, J. (1997). *Econometric Methods* (4th ed.). New York: McGraw- Hill Companies.

Judge, G.G., Hill, R.C., William, E., Lütkepohl, H. and Lee, T.C. (1982). *Introduction to the Theory and Practice of Econometrics*. New York: John Wiley & Sons.

Koepke, R. (2019). What drives capital flows to emerging markets? A survey of the empirical literature. *Journal of Economic Surveys*, 33(2), 516-540.

Kozłowska, M. (2015). Problems connected with measuring risks of foreign direct investments. *Journal of Economics & Management*, (20), 93-105.

Kusek, P., & Silva, A. (2017). What Matters to Investors in Developing Countries: Findings from the Global Investment Competitiveness Survey. Global Investment Competitiveness Report 2017/2018, 19.

Loungani, P., & Razin, A. (2001). How Beneficial is Foreign Direct Investment for Developing Countries? *Finance and Development*, 38: 6–9.

Mateev, M., & Stoyanov, I. (2014). Country Risk and Its Impact on Foreign Direct Investment Decision Making Process: A Bulgarian Perspective. *Oxford Journal: An International Journal of Business & Economics*, 6(1): 16-40.

Meldrum, D. (2000). Country risk and foreign direct investment. *Business economics*, 35(1), 33-40.

Omankhanlen, A. E. (2011). The Effect of Exchange Rate and Inflation on Foreign Direct Investment and its relationship with Economic Growth in Nigeria. *Economics and Applied Information* 1: 5–16.

Petrovic, E & Stankovic, J. (2009). Country Risk and Effects of Foreign Direct Investment. *Economics and Organization*. 6(1): 9 – 22.

Ramcharran, H. (1999). Foreign direct investment and country risk: Further empirical evidence. *Global Economic Review*, 28(3), 49-59.

Rejda, G. E. (2014). *Principles of Risk Management and Insurance*. Twelfth Edition. Pearson, New York.

Rodriguez, N. D. (2016). Country risk in foreign direct investment: similarities and differences with country risk in exports. *Nómadas. Critical Journal of Social and Juridical Sciences*, 49: 1-17

Sârbu, M. R. (2014). Forms and Motivations of Foreign Direct Investment. *SEA: Practical Application of Science*, 2(1).

Savoiu, G., Dinu, V., & Ciuca, S. (2013). Foreign direct investment based on country risk and other macroeconomic factors. Econometric models for Romanian economy. *Romanian Journal of Economic Forecasting,* 16(1), 39-61.

Schnitzer, M. (2002). Debt v. foreign direct investment: the impact of sovereign risk on the structure of international capital flows. *Economica*, 69(273), 41-67.

Sichei, M. M., & Kinyondo, G. (2012). Determinants of foreign direct investment in Africa: a panel data analysis. *Global Journal of Management and Business Research*, 12(18).

Topal, M., & Gul, O. (2016). The Effect of Country Risk on Foreign Direct Investment: A Dynamic Panel Data Analysis for Developing Countries. *Journal of Economics Library*, 3(1), 141-155.

Verbeek, M. (2004). *A Guide to Modern Econometrics (2nd ed.)*. England: John Wiley & Sons.

Vernon, R. (1966). International Investment and International Trade in the Product Cycle. *Quarterly Journal of Economics*, 88: 190 -207.

Williams, M. L. (1975). The extent and significance of the nationalization of foreign-owned assets in developing countries, 1956-1972. *Oxford Economic Papers*, 27(2), 260-273.

Zhang, Y. (2010). Sovereign Risk Management in Recession: The Cases of Sweden and China. Available at SSRN 1620554.

Farah Mohammadi (Author) *Toronto Metropolitan Univeristy* **Arghavan Asad (Co-Author)** *Toronto Metropolitan Univeristy* **Seham Al Abdul Wahid (Co-Author)** *Toronto Metropolitan Univeristy*	**Quantum Combinational Circuits Design: Python Approach.**

Abstract

As the demands for high performance, energy efficiency, and large bandwidth in artificial intelligence (AI) algorithms increase, quantum computing emerges as a promising solution to address the limitations of classical computing architectures. This paper presents the design and analysis of quantum combinational circuits which include half adders, full adders and ripple carry adders, implanted using IBM's Qiskit library on Python. Quantum computing leverage the principles of quantum mechanics, such as superposition and entanglement, to perform parallel computations and potentially provide exponential speedup for arithmetic operations. Quantum half adders are used as the basis for building full adders and ripple carry adders. Toffoli and CNOT quantum gates are used to optimize quantum cost and delay. Future work includes optimizing circuit efficiency and exploring alternative adder architectures to enhance the practicality and scalability of quantum computing applications in solving computational problems.

Keywords: Quantum Computing, Combinational Circuits Design, Quantum Gates, Quantum Circuits, Adders, Python Libraries

I. INTRODUCTION

As artificial intelligence (AI) algorithms evolve, new technologies that meet the high performance, energy efficiency and large bandwidth requirements are required. Von Neumann computers are widely used for running complex AI algorithms, which are based on an architecture where instructions and data share a common memory and are processed sequentially by a central processing unit (CPU). CPUs include a control unit and an arithmetic logic unit (ALU) [1, 2, 3, 4]. Quantum computers are non Von Neumann computers and can be used to overcome the current challenge classical machine learning (ML) algorithms are facing which is the increased demand for energy and computational power, particularly in handling large datasets. Quantum computing (QC), based on the principles of quantum mechanics, has the potential to contribute to the advancement of AI by providing exponential speedup of certain computations. In QC, information is represented using quantum bits, also known as qubits, which use the principle of superposition to simultaneously exist in multiple states of 0 and 1. This phenomenon provides quantum computers with the advantage of parallel computations on different possibilities, thus providing exponential speedup [5, 6, 7].

Adders in digital circuits are essential operators for many algorithms. Classical adders sequentially perform arithmetic operations on binary logic (0s and 1s) using logic gates. While quantum adders rely on qubits and quantum gates to perform parallel processing of multiple states simultaneously. Developing quantum counterparts to classical arithmetic operations, like those performed by half adders, full adders and ripple carry adders is crucial for reducing computational complexity, improving efficiency of quantum algorithms such as Shor's algorithm for factoring large numbers or Grover's search algorithm and improving scalability. In addition, it can be used for applications such as quantum cryptography and cybersecurity which are based on encryption and decryption algorithms that use arithmetic operations [8].

This paper proposes quantum circuit half adder, full adder and ripple carry adders designs. They are implemented and analyzed on python using the Qiskit library designed by IBM. Qiskit is a cloud-based, open access platform to real quantum computers with 5 or 16 qubits. In addition, it contains a 32 qubit cloud-based simulator [9].

II. BACKGROUND

Quantum computing is based on the quantum physics principles superposition, entanglement and quantum measurement (to process data). Superposition allows the qubits to exist in several states simultaneously [10]. Entanglement is the phenomenon where qubits become correlated with each other in such a way that the state of one qubit directly influences the state of another, regardless of the physical distance between them. This property enables the creation of highly interconnected quantum systems [5]. Quantum measurement is the process that transforms quantum information into classical information, which is essential for analysis by classical algorithms and computers [10].

A. Qubit

Qubit is the equivalent of a bit in classical computers, except they exist in a superposition state and is the fundamental unit of quantum information. It is denoted by Dirac notation as shown in equation 1 [6].

$$|0\rangle = \binom{1}{0}, \ |1\rangle = \binom{0}{1} \qquad (1)$$

Equation 2 represents the superposition state of qubits and is used to determine the final state of the qubit. As the qubit is measured, it will hold only one state, either state $|0\rangle$ with probability $|\alpha|2$ or state $|1\rangle$ with probability $|\beta|2$ [6].

$$|\psi\rangle = \alpha|0\rangle + \beta|1\rangle = \binom{\alpha}{\beta} \qquad (2)$$

B. Quantum Gates

Quantum Gates are the building blocks of quantum circuits, and they operate on the qubits to transform one quantum state into another quantum state. They are comparative to classical logic gates for conventional digital circuits, except quantum gates are all reversible. Due to this reversible property, quantum gates must always have the same number of inputs and outputs [6]. Quantum circuit diagrams are built and read from left to right where each line represents a circuit wire. The left side of the wire indicates the initial state of the qubit. The qubit remains in the same state until an operator is added to the same line of wire [10].

C. Types of Classical Adders

A classical half adder circuit includes two inputs, A and B and performs the computation of A+B. It has two outputs: S, which contains the least significant digit of the addition ($S=A\oplus B$) and Cout, which contains the most significant digit (Cout=AB). A full adder has three inputs: A, B and Cin, where Cin is the carry in bit. It will have S and Cout as outputs as well where $S=A\oplus B\oplus Cin$ and Cout=AB + ACin + BCin. Ripple carry adders is a type of carry propagate adders which are able to sum two N-bit numbers A and B with a carry in, and result in an output of N-bit number S and carry out. The carry out of every pair of bits Ai and Bi is propagated into the next pair of Ai+1 and Bi+1. Ripple carry adders is a chain consisting of N full adders, connecting the Cout output of every full adder with the Cin input of the next full adder [11].

III. QUANTUM ADDERS IMPLEMENTATION & ANALYSIS

A. Quantum Half Adder

A quantum half adder can be built using a Toffoli and CNOT quantum gates. Toffoli gates are three-qubit gates that can be used to compute Cout=AB. CNOT is a two-qubit gate that can compute S=A⊕B [11].

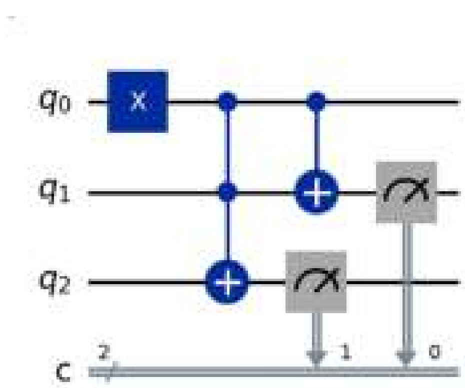

Fig 1. Half Adder Quantum Circuit

In Figure 1, q0 represents A, and q1 represents B. A is set to |1⟩ using the "X' gate, also known as Pauli-X Gate that is equivalent to a NOT gate, mapping the initial state of |0⟩ to a |1⟩. B is equivalent to |0⟩, as no quantum gate is applied to change its state. The next step of the circuit is the Toffoli gate, connecting inputs A and B to an auxiliary qubit q2 to compute Cout. The additional q2 qubit is used as a Toffoli gate operates on three qubits. The last step is the application of the CNOT gate between inputs A and B to calculate S. The measured output results in S=1 and Cout=0, as expected based on the inputs [6].

The code implementation of this circuit involves importing the Qiskit library on Python, followed by importing the required modules such as "QuantumCircuit" and "QuantumRegister". The "ccx" function is used to apply a Toffoli gate to the specified qubits, and "cx" is used to apply a CNOT gate. To initialize a qubit to a state of |1⟩ using the Pauli-X gate, the function "x" is used. Acquiring measurements of the output state of the qubits is completed using the "measure" function and mapping the desired qubit to a classical bit. Classical bits are initialized by defining a "ClassicalRegister", in a similar manner to defining a "QuantumRegister" [12].

Identifying the quantum cost of a circuit refers to the number of gates or quantum operations that are required to implement the circuit. However, each type of gate has its own cost associated with it. Quantum cost can be used as an indicator of efficiency and complexity, the lower the cost the more efficient and less complex the circuit is. The half adder includes two measure gates which are used to convert quantum information into classical bits, representing the sum and carry out results. Each measure gate has a quantum cost of 1. The x gate and cx gate each have a quantum cost of 1, while the ccx gate has a quantum cost of 5 as it involves more qubits. Thus, the total quantum cost of the half adder circuit adds up to 9. The total quantum cost can be reduced if both inputs are initialized to 0, which eliminates the x gate. In addition, the measurement operators may not always be necessary depending on the type of analysis that is required from circuit [13].

Another metric used to identify a quantum's circuit complexity is quantum delay which refers to the longest path of sequential gate operations on any qubit in the circuit. The half adder has a quantum delay of 3 [14]. The additional qubit added for intermediate calculations or storing temporary information are referred to as ancilla inputs [15]. While the qubits that contain some intermediate data that is not part of the desired output and no longer useful after the computation are called garbage outputs [16]. The designed half adder contains 1 ancilla input and 0 garbage outputs.

B. Quantum Full Adder

A quantum full adder can be built using three half adders. It first applies a CNOT gate between A and an auxiliary qubit, as well as between B and an auxiliary qubit. This will compute S1 and S2. The next step is applying the Toffoli gate between A, B and the auxiliary qubit to compute for Cout1. The previous steps illustrate the first two half adders, the third half adder is used to combine the outputs of the first two half adders and provide the final output. Figure 2 illustrates the full adder circuit with the inputs set to A=1, B=0 and Cin=1, resulting in an output of S=0 and Cout=1, as expected from the inputs.

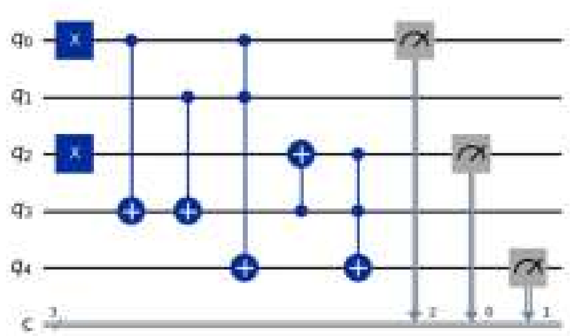

Fig 2. Quantum Full Adder Circuit

The gates used for a full adder are the same as a half adder circuit, however, more gates are used to accommodate for the operations. The full adder circuit has a quantum cost of 15, quantum delay of 3, 1 ancilla input and 0 garbage outputs.

C. Ripple Carry Adder

The ripple carry adder quantum circuit comprises of a sequence of full adder circuits connected in series that take the carry out from each full adder as the carry in of the next full adder. The number of full adders required is based on the number of bits of each input. For example, figure 3 illustrates the ripple carry adder of inputs A=101 and B=011, with Cin initialized at 0. Therefore, three full adders are required to compute the outputs. The first step takes A=1 and B=1, starting from the least significant bits (right), into the first full adder, resulting in an output of S=0 and Cout=1. The next step takes A=0 and B=1 with Cin equating to Cout=1 from the previous step into the second full adder. The output of the second step is S=0 and Cout=1. The last step takes A=1 and B=0 with Cin= Cout=1 into the third full adder. The output of the third step is S=0 and Cout=1. Thus, the final output of all three full adders is S=000 and Cout=1000.

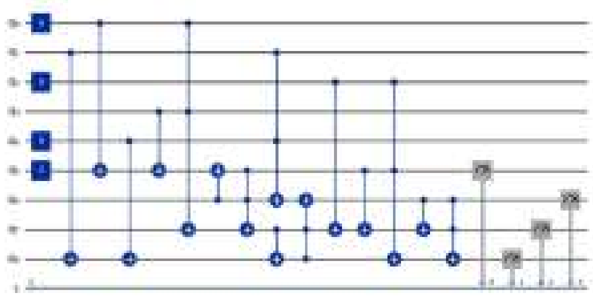

Fig 3. Ripple Carry Adder Quantum Circuit

The ripple carry adder is the most complex compared to previous adders as it implements three full adders in sequence to add two 3-bit numbers. The complexity of this circuit will increase as the number of input bits increases. The ripple carry adder has a quantum cost of 40, a quantum delay of 5, 2 ancilla inputs and 0 garbage outputs as qubits were either inputs or measured.

IV. CONCLUSION

This paper demonstrates the implementation and analysis of quantum adders, including half adders, full adders, and ripple carry adders, using the Qiskit Python library. Quantum computing offers a promising alternative to classical computing, with its potential for exponential speedup and parallel processing. Quantum adders, crucial for arithmetic operations in quantum algorithms, can significantly impact the performance of quantum computations.

Future research should explore further techniques to reduce quantum cost and delay of quantum adders which can also enhance the scalability of quantum adders and allow them to handle larger bit-widths without compromising efficiency or increasing complexity. Further adder architectures should be investigated to improve performance and reduce quantum resource usage. Lastly, the impact of optimized quantum adders can be assessed on the performance of key quantum algorithms such as Shor's algorithm for factoring and Grover's search algorithm.

REFERENCES

[1] A. Abdul, A. Asad, and F. Mohammadi, "A Survey on Neuromorphic Architectures for Running Artificial Intelligence Algorithms," Electronics, vol. 13, no. 15, pp. 2963–2963, Jul. 2024, doi: https://doi.org/10.3390/electronics13152963.

[2] Asad, A.; Kaur, R.; Mohammadi, F. A Survey on Memory Subsystems for Deep Neural Network Accelerators. Future Internet 2022, 14, 146. https://doi.org/10.3390/fi14050146.

[3] Asad, A.; Mohammadi, F. NeuroTower: A 3D Neuromorphic Architecture with Low-Power TSVs. In Lecture Notes in Networks and Systems; 2022; pp. 227–236. https://doi.org/10.1007/978-3-031- 18344-7_14.

[4] Kaur, R.; Asad, A.; Mohammadi, F. A Comprehensive Review on Processing-in-Memory Architectures for Deep Neural Networks. Computers 2024, 13, 174. https://doi.org/10.20944/preprints202406.1486.v1.

[5] R. Gupta et al., "Silicon Photonics Interfaced with Microelectronics for Integrated Photonic Quantum Technologies: A New Era in Advanced Quantum Computers and Quantum Communications?," Nanoscale, Dec. 2022, doi: https://doi.org/10.1039/D2NR05610K.

[6] Y. Zhang and Q. Ni, "Recent advances in quantum machine learning," Quantum Engineering, vol. 2, no. 1, Mar. 2020, doi: https://doi.org/10.1002/que2.34.

[7] Y. Zhu and K. Yu, "Artificial intelligence (AI) for quantum and quantum for AI," vol. 55, no. 8, Jun. 2023, doi: https://doi.org/10.1007/s11082-023-04914-6.

[8] C. Clear et al., "Optical transition parameters of the silicon T centre," arXiv (Cornell University), May 2024, doi: https://doi.org/10.48550/arxiv.2405.07144.

[9] S. Simmons, "Scalable Fault-Tolerant Quantum Technologies with Silicon Color Centers," PRX quantum, vol. 5, no. 1, Mar. 2024, doi: https://doi.org/10.1103/prxquantum.5.010102.

[10] A. Zeguendry, Z. Jarir, and M. Quafafou, "Quantum Machine Learning: A Review and Case Studies," Entropy, vol. 25, no. 2, p. 287, Feb. 2023, doi: https://doi.org/10.3390/e25020287.

[11] F. Orts, G. Ortega, E.F. Combarro, and E.M. Garzón, "A review on reversible quantum adders," Journal of Network and Computer Applications, vol. 170, pp. 102810–102810, Nov. 2020, doi: https://doi.org/10.1016/j.jnca.2020.102810.

[12] P. N. Singh and S. Aarthi, "Quantum Circuits – An Application in Qiskit-Python," IEEE Xplore, Feb. 01, 2021. https://ieeexplore.ieee.org/document/9388498

[13] Md. Selim, “Quantum Cost Optimization for Reversible Sequential Circuit,” International Journal of Advanced Computer Science and Applications, vol. 4, no. 12, 2013, doi: https://doi.org/10.14569/ijacsa.2013.041203.

[14] Majid Haghparast and A. Bolhassani, “Optimized parity preserving quantum reversible full adder/subtractor,” International journal of quantum information, vol. 14, no. 03, pp. 1650019–1650019, Apr. 2016, doi: https://doi.org/10.1142/s0219749916500192.

[15] T. Proctor and Viv Kendon, “Hybrid quantum computing with ancillas,” Contemporary Physics, vol. 57, no. 4, pp. 459–476, Mar. 2016, doi: https://doi.org/10.1080/00107514.2016.1152700.

[16] A. A. Saki, M. Alam, K. Phalak, A. Suresh, R. O. Topaloglu, and S. Ghosh, “A Survey and Tutorial on Security and Resilience of Quantum Computing,” IEEE Xplore, May 01, 2021. https://ieeexplore.ieee.org/document/9465397

Momoiyioluwa Oluyemi (Author)
University of Waterloo

Pranav Agrawal(Co-Author)
University of California Los Angeles

Armaghan Salehian (Co-Author)
University of Waterloo

Optimal Cable Wrapping Patterns for Minimizing Dynamic Impacts on a Host Plate Structure

Abstract

Multiple studies have shown that the power and signal transmission cables present in lightweight engineering structures significantly alter the dynamic behaviour of these structures. The objective of this work is to determine the optimal cable placement geometry on a host plate structure such that its dynamic behaviour undergoes minimal changes upon attachment of the cables. The cable wrapping is assumed to be periodic such that the cable-harnessed structure consists of several repeating fundamental elements. This allows for the application of an energy-equivalence homogenization approach for the development of the analytical model so that the optimization can be carried out. An optimization algorithm is used to check how well the frequency response functions of several cable-harnessed plate structures match that of the corresponding plate with no cables attached, to determine the ones that were least impacted by the cables attached to them.

Keywords:

Vibrations, Structural Dynamics, Continuum Modeling, Cable-Harnessed Structures, Plate Structures, Homogenization Method, Optimal Cable Wrapping, Natural Frequency, Frequency Response Function

1 Introduction

Several modern engineering structures consist of cables as an integral part of their design, particularly for the purpose of signal and power transmission. These cables can have an adverse effect on the structure's dynamic response and properties, especially when they account for a significant portion of the total mass of the structure. It is therefore important to have models that can accurately predict the effect of the cables on the host structure to which they are harnessed. In particular, these models can pave the way to finding potential solutions for the optimal placement of the cables that minimizes their impact on the dynamic response and properties of the host structure. Such solutions are greatly beneficial because it means that the effects of the cables will not have to be considered in a dynamic analysis of the cable-harnessed structure, greatly simplifying the models applied to it.

Recent successful efforts have been made into the development of accurate analytical models for cable-harnessed structures. Attempts at creating a model for a host structure with cables wrapped around it were first made on a host beam structure. Because of the complex nature of this kind of structure, the cable wrapping was assumed to be done in a periodically repeated manner to simplify the problem so that an energy-equivalence homogenization approach could be used in the model development (Martin and Salehian, 2013, 2016a, 2016b). Martin and Salehian, 2016a, however do consider the longitudinal cable placement as a special case. To further generalize the wrapping configuration, a semi periodic cable wrapping around the host beam was studied, which led to the development of a spatially dependent analytical model for such a cable-harnessed structure (Martin and Salehian, 2019). These works did not consider the damping effects of the added cables, thus, Agrawal and Salehian, 2021a, 2021b, sought to fill this gap by incorporating Kelvin-Voigt and hysteretic energy loss mechanisms into the model for a periodically-wrapped beam structure.

The study of beam structures was the first step towards developing accurate models for cable-harnessed structures be cause of their one-dimensional nature. As a next step, models have been developed for host plate structures, which have the characteristic of being two-dimensional and hence applicable to modeling a wider range of engineering structures. Again, for the sake of simplicity, developments so far for this type of cable-harnessed structure have been focused on structures for which the wrapping configuration can be viewed as being periodically repeated in some type of way, so that the energy-equivalence homogenization approach can be applied. A plate structure with cables placed parallel to one of its edges was first studied (Agrawal and Salehian, 2021c) after which an analytical model for periodically wrapped plate structures was created (Agrawal and Salehian, 2021d, 2022).

Analyses carried out in the aforementioned works show that the harnessing of cables to a host structure clearly has notable effects on the dynamic properties of the structure. This naturally serves as motivation to investigate the pos sibility of the existence of an optimal wrapping pattern for which the harnessing of the cables has little to no impact on the host structure's dynamics. Such a work has been carried out by Cao et al., 2021, for a host beam structure, where the analytical model for periodically-wrapped cable-harnessed beams developed by Martin and Salehian, 2013, 2016a, 2016b, was applied to find the optimal solutions. The aim of the work presented in the current document is to do the same for a host plate structure, as no prior studies have carried out this work. The already developed model for periodically-wrapped plate structures in the works by Agrawal and Salehian, 2021d, 2022, is used.

2 Analytical Model and Optimization Procedure

This section presents the crucial details of the continuum modeling for the cable-harnessed plate structure and elu cidates the optimization methodology. The analytical cable-harnessed plate model employed for the optimization in this paper was developed by Agrawal and Salehian, 2021d, and their paper provides a comprehensive derivation of the model.

2.1 Analytical Model

The method of energy-equivalence homogenization is utilized to formulate the mathematical model of the cable harnessed plate structure with periodic wrapping. This wrapping allows the plate to be viewed as being composed of fundamental elements, repeated in orthogonal directions, which constitute the entire structure. The homogenization approach leverages this periodicity to create an energy-equivalent continuum model. The first step is calculating the strain and kinetic energy of the structure's fundamental element, and then determining its energy per unit area. The central assumption of the homogenization method is that the energy densities calculated for a single element accu rately represent the strain and kinetic energy densities of the whole structure. This leads to an equivalent homogenized continuum plate with multiple elements. Subsequently, the total homogenized strain and kinetic energy are computed and used to derive the governing equation of motion in the structure's transverse vibration coordinate using Hamilton's principle.

Figure 1 presents a schematic of the cable-harnessed system studied in this work. The cables are periodically wrapped around a thin rectangular plate with dimensions $a \times b \times h$. The plate is modeled using classical plate theory, suitable only for thin plates, thus the thickness h is much smaller than both the length a and the width b. The structure's fundamental element is sized $L_1 \times L_2 \times h$, with its dimensions dependent on the number of fundamental elements per row, μ, and the total number of rows, η. These parameters also define the wrapping angle θ, measured in relation to the direction of wrapping. As depicted in Figure 1, the cables are assumed to be wrapped in the direction of the x-axis. For the structure displayed in the figure, $\mu = 3$ and $\eta = 2$. Given that $L_1 = \frac{a}{\mu}$ and $L_2 = \frac{b}{\eta}$, the wrapping angle is determined by the following expression (Agrawal and Salehian, 2021d):

$$\mathbf{Tan\theta} = \frac{2L2}{L1} = \frac{2b\mu}{a\eta}$$

The development of the continuum model is based on multiple assumptions. Given that classical plate theory is employed to model the plate, plane stress conditions are assumed. The material of the plate is considered homogeneous and isotropic. The cable, with a circular cross-section, is under a pre-tension T in the equilibrium state of the system, resulting in compression and shear forces in the plate. It is presumed that the cable maintains perfect contact with the plate throughout the vibrations, and that the axial strain in the cable is uniform across any given cross-section.

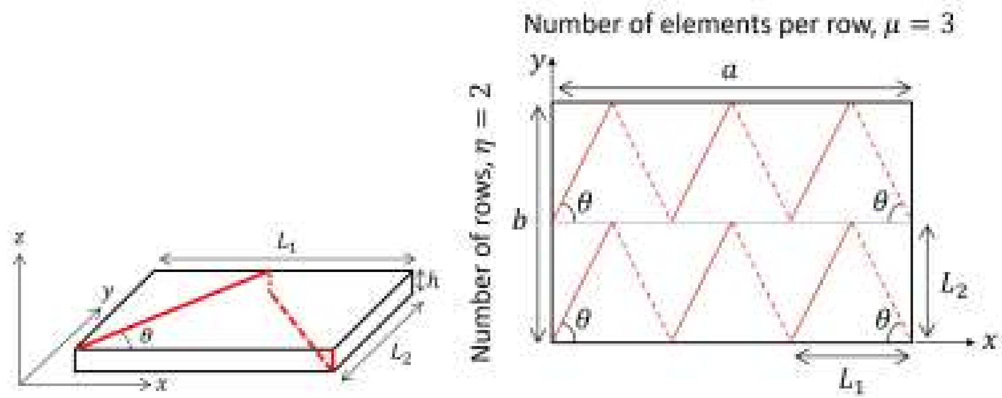

(a) Fundamental element (b) Periodically-wrapped plate

Figure 1: Schematic of cable-harnessed plate structure. The red lines represent the cables. The solid lines represent the segments of the cables on the top surface of the plate while the dashed lines represent the parts on the bottom surface.

According to Agrawal and Salehian, 2021d, the total homogenized strain energy of the cable-harnessed plate structure can be expressed as

$$U = \frac{1}{2}\int_0^b \int_0^a \big(H_1 + H_2 w_{,xx}^2 + H_3 w_{,yy}^2 + H_4 w_{,xy}^2 + H_5 w_{,x}^2 + H_6 w_{,y}^2 - H_7 w_{,xx} + H_8 w_{,xy} - H_9 w_{,yy} + H_{10} w_{,xx} w_{,xy} + H_{11} w_{,yy} w_{,xy} + H_{12} w_{,x} w_{,y} + H_{13} w_{,xx} w_{,yy}\big)\, dx\, dy, \quad (2)$$

and the total homogenized kinetic energy as

$$T = \frac{1}{2}K_1 \int_0^b \int_0^a \dot{w}^2\, dx\, dy. \quad (3)$$

The subscript following the comma denotes spatial differentiation with respect to the indicated variable(s). The over dot signifies time differentiation. The homogenized coefficients are expressed in terms of the system parameters in the Appendix. The coefficient K_1 from the kinetic energy denotes the system's mass per unit area. Employing the homogenized energy expressions from Equations (2) and (3), Hamilton's principle is utilized to ascertain the system's dynamic behavior. Consequently, the governing equation of motion for the equivalent continuum cable-harnessed plate is derived as

$$H_2 w_{,xxxx} + H_3 w_{,yyyy} + (H_4 + H_{13}) w_{,xxyy} + K_1 \ddot{w} = 0 \quad (4)$$

The coefficients H_2 and H_3 denote the bending stiffness of the homogenized system in the x and y directions, respec tively. H_4 represents the twisting stiffness, while H_{13} signifies the coupled bending stiffness in the x and y directions.

This study concentrates on the clamped-free-free-free (CFFF) boundary conditions, corresponding to a cantilevered plate. Given these boundary conditions, the governing equation of motion (4) cannot be solved in closed form. There fore, the Rayleigh-Ritz method (Meirovitch, 1975; Young, 1950), an approximate analytical technique, is utilized to determine the system's natural frequencies, mode shapes, and frequency response functions. The method involves using 36 trial functions derived from the assumed mode shape functions of a clamped-free and free-free beam to ap proximate the solution to the eigenvalue problem associated with the cable-harnessed system with CFFF boundary conditions.

2.2 Optimization Procedure

The dynamic effects introduced by adding cables to the host plate structure can be observed through frequency response function (FRF) plots of the cable-harnessed system versus the system without cables. This is because FRFs reflect the dynamic characteristics and the response of a system to external excitations. Consequently, the aim of this optimization effort is to identify cable wrapping patterns on the plate that result in an FRF for the plate with cables (the cabled plate) that closely resembles the FRF of the plate without cables (the bare plate). Achieving this would imply that the dynamic behavior of the bare and cabled plates is nearly identical, despite the addition of cables. The search for these optimal wrapping patterns starts with establishing an appropriate objective function.

The clearest method to establish the objective function for optimization is to create a function aimed at minimizing the differences between the natural frequencies of cabled and bare plates, similar to the approach used by Cao et al., 2021, for beam structures. However, since the aim here is to align the frequency response functions of these structures, and considering the absence of an exact closed-form solution, solely reducing the natural frequency differences is inadequate. Therefore, the differences in the anti-resonant frequencies must also be minimized. To enhance accuracy, a third minimization criterion is introduced: the disparities in the FRF amplitude values. This is because it is possible to have an FRF plot where the natural and anti-resonant frequencies align, yet there is a vertical discrepancy in the plots due to variations in the FRF amplitudes at each frequency. Such discrepancies would not be addressed by only minimizing natural and anti-resonant frequencies. Consequently, the objective function is defined to include these considerations. It is expressed as :

$$f(\mu,\eta) = c_1\sqrt{\frac{1}{m}\sum_{i=1}^{m}\left(\frac{\omega_{n,i}^{\mathrm{cp}}-\omega_{n,i}^{\mathrm{bp}}}{\omega_{n,i}^{\mathrm{bp}}}\right)^2} + c_2\sqrt{\frac{1}{n}\sum_{j=1}^{n}\left(\frac{\omega_{\alpha,j}^{\mathrm{cp}}-\omega_{\alpha,j}^{\mathrm{bp}}}{\omega_{\alpha,j}^{\mathrm{bp}}}\right)^2} + c_3\sqrt{\frac{1}{r}\sum_{k=1}^{r}\left\{\frac{\log\left[\gamma^{\mathrm{cp}}(\omega_k)\right]-\log\left[\gamma^{\mathrm{bp}}(\omega_k)\right]}{\log\left[\gamma^{\mathrm{bp}}(0)\right]}\right\}^2}. \quad (5)$$

Equation (5) above is a weighted average of the root mean square (RMS) values representing each of the minimization criteria described earlier. The superscripts 'cp' and 'bp' denote 'cabled plate' and 'bare plate,' respectively. The symbol ω_n denotes natural frequency, while ω_α denotes anti-resonant frequency. The frequency response function is denoted by $\gamma(\omega)$, and its logarithm is utilized in the RMS calculation because the FRF's vertical axis features a logarithmic scale. Each term's division serves as normalization relative to the bare plate. The optimization problem's decision variables are the wrapping pattern parameters, namely the number of fundamental elements per row, μ, and the number of rows, η, which determine the structure's periodicity. As illustrated by Equation (1), the parameters in question are associated with the cable wrapping angle, which consequently has a direct impact on the degree to which the cables modify the dynamics of the host structure. Being required to be positive integers, they must adhere to the subsequent relation, serving as a constraint within this optimization problem:

$$(\mu,\eta) \in \mathrm{N}^2, \quad (6)$$

where N denotes the set of natural numbers. The objective is to identify the pairs of μ and η that comply with the constraint (6) and yield the minimum values of the objective function (5).

3 Results and Discussion

We place our focus on a specific cable-harnessed plate structure; that is, all system parameters remain constant except for the cable wrapping pattern parameters μ and η. The system parameters employed are identical to those used by Agrawal and Salehian, 2021d, detailed in Table 1. These parameters represent an aluminum plate and Power Pro cables. It is also established that this study is limited to CFFF boundary conditions, with the clamped condition consistently applied along the edge at $x = 0$.

The parameters of the wrapping pattern that result in minimal cable dynamic impact were determined by evaluating various μ-η combinations that meet the restriction outlined by Equation (6). The output values from the objective function (5) for these combinations were then compared to identify the pairs yielding the lowest values. All calculations were conducted within the 0-500

Hz frequency range. Consequently, for the natural and anti-resonant frequencies, only those within this range were utilized for the RMS calculations in the objective function. The FRF amplitudes were also computed solely for this frequency range. The actuation location for the FRF amplitude computations was set at (0.1*a*, 0.8*b*), and the sensing location at (0.4*a*, 0.8*b*), relative to the origin, following the methodology of Agrawal and Salehian, 2021d. Equal weights of $c_1 = c_2 = c_3 = \frac{1}{3}$ were employed for the weighted average. The mode shapes within the frequency range of interest are depicted in Figure 2. It has been observed that the mode shapes remain consistent for the plate with and without cables, suggesting that the addition of cables does not influence the mode shapes of the

Table 1: Material and geometric properties of the cable-harnessed plate structure as used by Agrawal and Salehian, 2021d

Plate
Length (a) 0.201 mWidth (b) 0.099 m Thickness (h) 0.0012 m Mass density (ρ_p) 2768 kg/m^3 Young's modulus (E_p) 68.9 GPa Poisson's ratio (v) 0.33
Cable
Radius (r_c) 0.55 mmYoung's modulus (E_c) 128 GPa Mass density (ρ_c) 1400 kg/m^3 Pre-tension (T) 3 N

(a) Mode 1 (b) Mode 2 (c) Mode 3 (d) Mode 4 (e) Mode 5

Figure 2: First five mode shapes of the cable-harnessed plate structure

host plate under these boundary conditions, at least for the first five modes. The 1st, 3rd, and 5th modes predominantly exhibit bending in the direction of the x-axis, while the 2nd and 4th modes are primarily characterized by twisting.

Upon applying the methodology described in the previous paragraph, we find that the dynamics of the host plate are minimally impacted when there is only one row of cable and a relatively small number of fundamental elements in the row. More specifically, $\mu \leq 7$ and $\eta = 1$ yield cabled-harnessed plate structures whose FRFs match very closely with that of the bare plate. Figure 3 shows the FRF of two cabled plate structures compared against that of the corresponding bare plate. The first structure is one onto which the cable is wrapped optimally, with $\mu = 5$ and $\eta = 1$. In the second cabled plate, $\mu = 3$ and $\eta = 5$. This represents the cabled plate structure studied extensively by Agrawal and Salehian, 2021d, upon development of the homogenized analytical model for cable-harnessed plates. It is clear that for the optimally wrapped plate, the impact of the cables is negligible as the FRF of the cabled plate aligns very well with that of the bare plate. This means that with this wrapping configuration applied, the strain and kinetic energy contributions of the cable nearly neutralize each other. In the second plate, the dominant stiffening effect of the cable, initially observed by Agrawal and Salehian, 2021d, is evident since all the natural frequencies increase upon harnessing of the cables onto the bare plate. Compared to the optimally wrapped structure, the increase in the natural frequencies whose associated modes shapes are x-direction bending dominant (Modes 1, 3 and 5), is as a result of an increase in the homogenized x-direction stiffness coefficient H_2, which occurs because of a decrease in the wrapping angle θ. For the modes with a dominant twist-like shape (Modes 2 and 4), an increase in the homogenized stiffness coefficient $(H_4 + H_{13})$ is what causes an increase in the corresponding natural frequencies for these modes.

4 Conclusion

This paper presents the identification of optimal cable pattern configurations for cable-harnessed plate structures, wrapped in a periodic manner, to minimize the cables' impact on the host plate's dynamics. Utilizing a previously developed analytical model based on energy-equivalent homogenization, a suitable objective function is established to determine these wrapping configurations. The study concludes that a cantilevered plate with one row and no more than seven fundamental elements per row experiences the least impact from the cables on its dynamics. These in

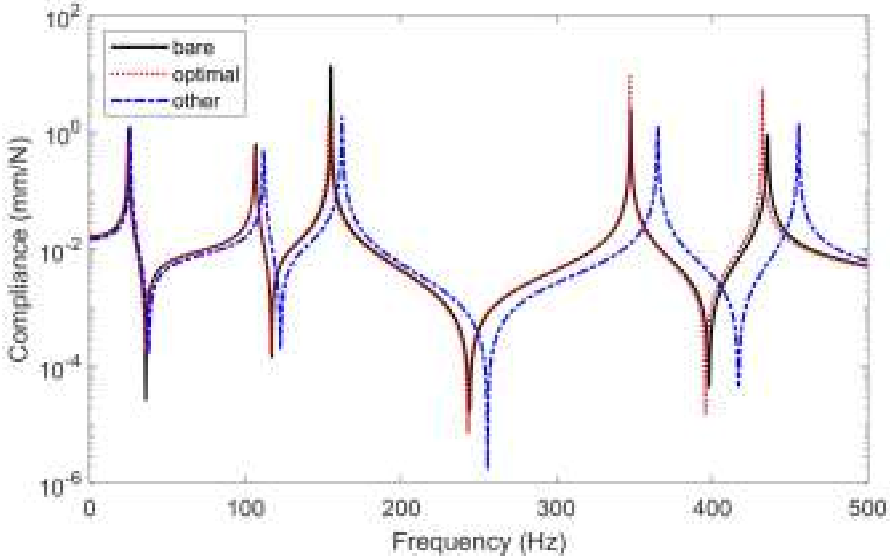

Figure 3: Comparison of frequency response functions of a bare plate and two cable-harnessed plates – one is optimally wrapped and the other is not

sights are significant for simplifying models in applications that involve attaching cables to plate-like structures, as they demonstrate that optimal cable placement can negate the need to consider the cable's effects on the host structure.

Appendix

Coefficients from the homogenized strain and kinetic energy expressions

$$K_1 = \rho_p h + \frac{\rho_c A_c}{L_2 \cos\theta} + \frac{2\rho_c A_c h}{L_1 L_2},$$

$$H_1 = \frac{T^2}{E_c A_c L_2 \cos\theta} + \frac{1}{hE_p}\left(N_x^2 + N_y^2 - 2\nu N_x N_y + 2(1+\nu)N_{xy}^2\right),$$

$$H_2 = D + \frac{E_c A_c z_c^2 \cos^3\theta}{L_2} + \frac{T z_c^2 \cos\theta}{L_2} + \frac{N_x h^2}{24}, \quad H_3 = D + \frac{E_c A_c z_c^2 \sin^4\theta}{L_2 \cos\theta} + \frac{T z_c^2 \sin^2\theta}{L_2 \cos\theta} + \frac{N_y h^2}{24},$$

$$H_4 = 2D(1-\nu) + \frac{4E_c A_c z_c^2 \cos\theta \sin^2\theta}{L_2} + \frac{T z_c^2}{L_2 \cos\theta} + \frac{N_x h^2}{24} + \frac{N_y h^2}{24},$$

$$H_5 = \frac{T\cos\theta}{L_2} + N_x = 0, \quad H_6 = \frac{T\sin^2\theta}{L_2\cos\theta} + N_y = 0, \quad H_7 = 0, \quad H_8 = 0, \quad H_9 = 0,$$

$$H_{10} = \frac{N_{xy} h^2}{6} = 0, \quad H_{11} = \frac{N_{xy} h^2}{6} = 0, \quad H_{12} = 2N_{xy} = 0, \quad H_{13} = 2\nu D + \frac{2E_c A_c z_c^2 \cos\theta \sin^2\theta}{L_2}.$$

The forces Nx, Ny, and Nxy represent uniformly distributed compressive loads in the x and y directions, respectively, and shear load per unit length across the plate's thickness, resulting from the cable pre-tension. They are given by

$$N_x = -\frac{\eta T \cos\theta}{b}, \quad N_y = -\frac{2\mu T \sin\theta}{a}, \quad N_{xy} = 0.$$

References

Agrawal, P., & Salehian, A. (2021a). Damping mechanisms in cable-harnessed structures for space applications: Ana lytical modeling. *Journal of Vibration and Acoustics*, *143*(2).
Agrawal, P., & Salehian, A. (2021b). Damping mechanisms in cable-harnessed structures for space applications: Ex perimental validation. *Journal of Vibration and Acoustics*, *143*(2).
Agrawal, P., & Salehian, A. (2021c). Vibrations analysis of cable-harnessed plates: Continuum modeling and experi mental validation. *Journal of Vibration and Acoustics*, *143*(5).
Agrawal, P., & Salehian, A. (2021d). Continuum modeling and vibration analysis of cable-harnessed plate structures of periodic patterns. *Journal of Vibration and Acoustics*, *143*(6).
Agrawal, P., & Salehian, A. (2022). Dynamic analysis and experimental validation of periodically wrapped cable harnessed plate structures. *Experimental Mechanics*, *62*(6), 909–927.
Cao, S., Agrawal, P., Qi, N., & Salehian, A. (2021). Optimal geometry for cable wrapping to minimize dynamic impacts on cable-harnessed beam structures. *Journal of Vibration and Acoustics*, *143*(4).
Martin, B., & Salehian, A. (2013). Dynamic modelling of cable-harnessed beam structures with periodic wrapping patterns: A homogenization approach. *International Journal of Modelling and Simulation*, *33*(4), 185–202. Martin, B., & Salehian, A. (2016a). Mass and stiffness effects of harnessing cables on structural dynamics: Continuum modeling. *AIAA Journal*, *54*(9), 2881–2904.
Martin, B., & Salehian, A. (2016b). Homogenization modeling of periodically wrapped string-harnessed beam struc tures: Experimental validation. *AIAA Journal*, *54*(12), 3965–3980.
Martin, B., & Salehian, A. (2019). Continuum modeling of nonperiodic string-harnessed structures: Perturbation theory and experiments. *AIAA Journal*, *57*(4), 1736–1751.
Meirovitch, L. (1975). *Elements of vibration analysis*. McGraw-Hill.
Young, D. (1950). Vibration of rectangular plates by the Ritz method. Journal of Applied Mechanics, 17,
448-453


GLOBAL
CONFERENCE ALLIANCE INC. ™
Global Conference Alliance Inc.
Please Take a minute &
Review Us on Google
GLOBAL
ACCREDITED BUSINESS
BBB Rating:
GREATER VANCOUVER BOARD OF TRADE
TORONTO REGION